

doi: 10.12029/gc20170406

洪俊, 计文化, 张海迪, 刘明义, 马中平, 李艳广, 张辉善. 2017. 帕米尔地区穆尔尕布辉长岩-闪长岩的成因: 锆石U-Pb年龄、Hf同位素及岩石地球化学证据[J]. 中国地质, 44(4): 722-736.

Hong Jun, Ji Wenhua, Zhang Haidi, Liu Mingyi, Ma Zhongping, Li Yanguang, Zhang Huishan. 2017. Petrogenesis of Murgab gabbro-diorite from Pamir: Evidence from zircon U-Pb dating, Hf isotopes and lithogeochemistry[J]. Geology in China, 44(4): 722-736(in Chinese with English abstract).

帕米尔地区穆尔尕布辉长岩-闪长岩的成因: 锆石U-Pb年龄、Hf同位素及岩石地球化学证据

洪俊^{1,2} 计文化² 张海迪² 刘明义² 马中平² 李艳广² 张辉善²

(1. 中国地质科学院, 北京 100037; 2. 中国地质调查局西安地质调查中心, 陕西 西安 710054)

提要: 穆尔尕布岩体位于塔吉克斯坦帕米尔地区中部, 中帕米尔和南帕米尔之间的Rushan-Pshart缝合带中, 岩石类型主要由辉长岩和少量闪长岩组成, 呈岩株状侵入于新元古代(?)萨雷吉尔加组浅变质碎屑岩中。根据LA-ICP-MS锆石U-Pb定年结果, 穆尔尕布岩体中辉长岩的年龄为(232.0±1.5)Ma, 闪长岩的年龄为(231.5±1.9)Ma, 两者在误差范围内一致, 代表了该岩体的形成时代。辉长岩和闪长岩中锆石的 $\varepsilon_{\text{Hf}}(t)$ 值变化范围分别为4.8~12.1、6.4~10, 加权平均值为8.1±1.5(MSWD=6.5)和7.9±0.8(MSWD=2.4), 显示其原岩来源于地幔物质, 其单阶段Hf模式年龄 T_{DM1} 分别为477~621 Ma, 391~672 Ma, 指示其原岩为寒武纪—前寒武纪基底。岩石地球化学研究表明, 辉长岩类具有贫碱、低Al、富Mg特征, 属于低钾(拉斑)系列, 闪长岩类则显示富Si、Al, 贫Mg、低Ti的特征, 属于钙碱性-高钾钙碱性系列; 两者的稀土和微量元素特征相似, 稀土总量高, 呈轻稀土富集的右倾型配分型式, 无Eu异常或轻微正Eu异常, 微量元素富集大离子亲石元素, 亏损高场强元素, 指示穆尔尕布岩体可能形成于岛弧环境。综合区域地质资料, 认为在晚三叠世Rushan洋陆俯冲尚未结束, 表明洋盆闭合时限晚于232 Ma。

关 键 字: 帕米尔; 穆尔尕布岩体; LA-ICP-MS锆石U-Pb年龄; 锆石Hf同位素

中图分类号:P588.12²; P588.12⁴; P597.3 文献标志码:A 文章编号:1000-3657(2017)04-0722-15

Petrogenesis of Murgab gabbro-diorite from Pamir: Evidence from zircon U-Pb dating, Hf isotopes and lithogeochemistry

HONG Jun^{1,2}, JI Wenhua², ZHANG Haidi², LIU Mingyi², MA Zhongping²,
LI Yanguang², ZHANG Huishan²

(1. Chinese Academy of Geological Sciences, Beijing, 100037, China;
2. Xi'an Center of China Geological Survey, Xi'an 710054, Shaanxi, China)

Abstract: Located in the central part of Pamir, Tajikistan, near the Rushan-Pshart suture zone, the Murgab pluton separates the middle Pamir from southern Pamir. Petrologically, the pluton consists of gabbro and diorite which intruded into the epimetamorphic

收稿日期:2017-07-19; 改回日期:2017-07-30

基金项目:中国地质调查局项目(121201112036、12120114018601)资助。

作者简介:洪俊,男,1985年生,博士生,工程师,研究方向:造山带岩浆作用研究及区域地质矿产调查;E-mail:hongjunmail2013@163.com。

detrital rocks of late Proterozoic (?). LA-ICP-MS zircon U-Pb dating shows that the age of gabbro and that of diorite is 232 ± 1.5 Ma and 231.5 ± 1.9 Ma respectively, which represents the formation age of this pluton. The $\epsilon_{\text{Hf}}(t)$ values of the zircon are in the range of 4.8–12.1 and 6.4–10, with a weighted average of 8.1 ± 1.5 (MSWD = 6.5) and 7.9 ± 0.8 (MSWD = 2.4), suggesting that its original rock was derived from mantle materials. The one-stage Hf model ages (T_{DMI}) are 477 – 621 Ma, 391 – 672 Ma respectively indicating an original rock of Cambrian–Precambrian basement. The lithogeochemical data shows that gabbros are characterized by rich Mg and, poor Al and alkali, thus belonging to low-potassium rocks, whereas the diorites are rich in Si, Al and poor in Mg, Ti, hence belonging to calc-alkaline to high K calc-alkaline rocks. The gabbros and diorites share similar REE and trace elements features, which are characterized by high total REE content and rich LREE with slight normal Eu anomaly. The trace elements are characterized by rich LILEs and poor HFSEs. Based on geochemical characteristics, the authors infer that the pluton formed in an island-arc environment. The subduction was continuing during late Triassic, which indicates that the Rushan Ocean basin was closed at least later than 232 Ma.

Key words: Pamir; Murgab complex; zircon LA-ICP-MS U-Pb dating; zircon Hf isotopes

About the first author: HONG Jun, male, born in 1985, doctor candidate and engineer, engages in the study of magmatism of orogenic belts and regional geology and mineral investigation; E-mail: hongjunmail2013@163.com.

Fund support: Supported by China Geological Survey Program (No. 121201112036, 12120114018601).

1 引言

帕米尔构造结位于青藏高原西北部,其经历了古生代和中生代的多期造山运动,新生代以来由于印度板块向欧亚板块俯冲碰撞而产生强烈的地壳缩短和隆升,形成向北突出的弧形造山带,是揭示青藏高原形成和演化历史的关键地区之一(Burtman and Molnar, 1993; Yin et al., 2000; Ducea et al., 2003)。帕米尔造山带通常分别以Tanymas、Rushan-Pshart缝合带为界划分为北帕米尔、中帕米尔和南帕米尔三个构造单元,后者又进一步划分为东南帕米尔和西南帕米尔(Burtman and Molnar, 1993; Robinson, 2014)。帕米尔地区沿主要缝合带保存了大量与特提斯洋构造演化有关的蛇绿岩和岩浆岩,但主要集中在北帕米尔和中帕米尔地体之间的Tanymas缝合带(Matte et al., 1996; Robinson et al., 2004, 2007, 2012; Schwab et al., 2004; Angiolini et al., 2013),对于Rushan-Pshart缝合带的属性和洋盆闭合时限仍存在争议。大多数学者认为Rushan-Pshart缝合带代表中帕米尔和南帕米尔之间的规模相对较小的局限洋盆,主要依据是缝合带两侧缺少大规模与俯冲相关的弧岩浆活动(Leven, 1995; Schwab et al., 2004; Burtman, 2010; Lukens et al., 2012; Angiolini et al., 2013)。关于Rushan洋盆的闭合时间,有学者认为在晚侏罗—早白垩世(Pashkov and Shvol'man, 1979; Burtman and Molnar, 1993;

Schwab et al., 2004),也有学者认为中、南帕米尔地体在晚三叠世(Angiolini et al., 2013)碰撞。

本文以中帕米尔地体南缘穆尔尕布辉长-闪长岩为研究对象,在详细的野外地质调查的基础上,通过对该杂岩体的岩石学、地球化学及锆石LA-ICP-MS法U-Pb定年和Hf同位素研究,结合区域研究资料,揭示其形成时代、岩石成因及其形成的大地构造背景,对于Rushan-Pshart洋盆闭合时限、青藏高原西北缘构造演化研究具有重要意义。

2 地质背景与岩石学特征

帕米尔地区地处中塔边界,主体在塔吉克斯坦境内,位于青藏高原的西北缘,是古亚洲构造域和特提斯构造域强烈叠加部位,构造形迹极其复杂,中新生代岩浆活动强烈,断裂构造发育(Ducea et al., 2003; 洪俊等, 2014, 2015)。研究区位于中、南帕米尔交界,中帕米尔出露晚元古代片岩、石英岩和大理岩,寒武系—泥盆系出露较全,主要为灰岩、泥岩、页岩,显示被动大陆边缘沉积组合特征。石炭系一下二叠统为砂岩、粉砂岩、灰岩及少量安山岩,不整合于早古生代地层之上,上三叠统一侏罗系为滨浅海相沉积岩石组合。

区内近东西走向的辉长岩-闪长岩带(图1),长近40 km,由20余个中基性岩体组成,单个岩体出露面积较小(图2a),为1~2 km²,呈串珠状分布,以辉长岩占主体,部分岩体中辉长岩与闪长岩在空间上

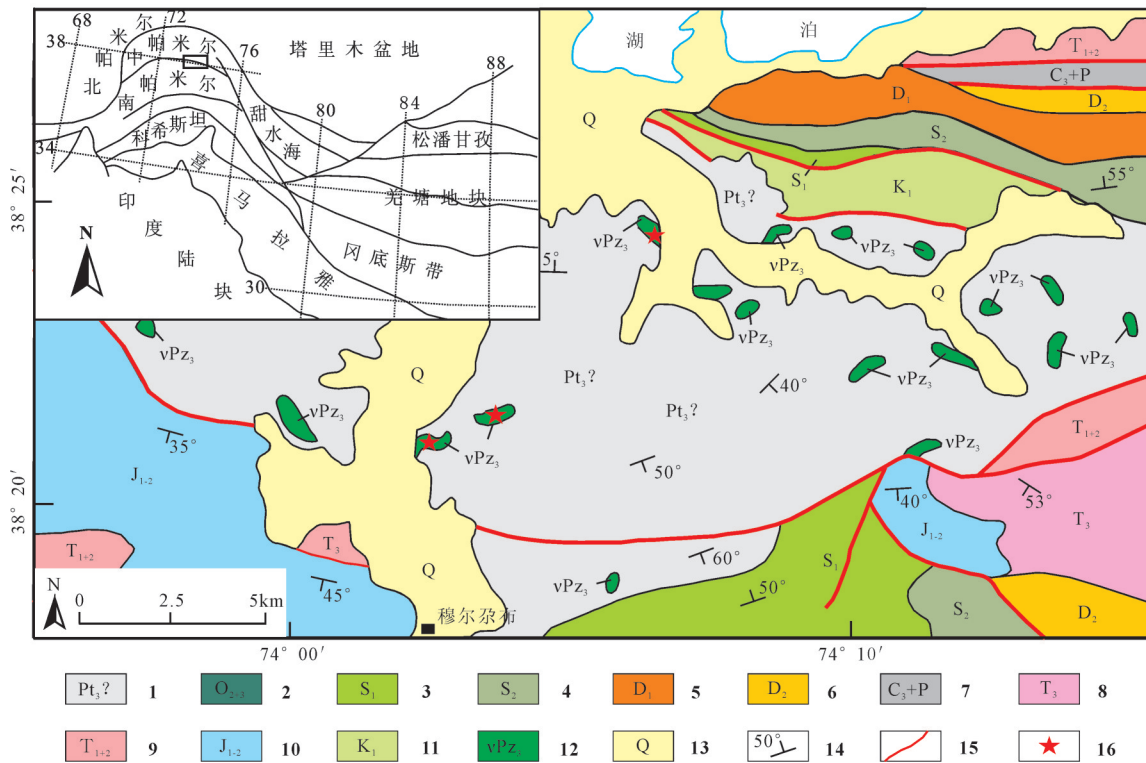


图1 东南帕米尔穆尔尕布地区区域地质图(据苏联1:20万地质图(1967)^①修改)

1—萨尔吉尔加组片岩,大理岩;2—拉克库里组页岩、砂岩和灰岩;3—下志留统灰岩、砂岩和火山岩;4—上志留统灰岩、页岩;5—下泥盆统灰岩;6—中泥盆统灰岩、白云岩;7—上石炭—二叠系灰岩、含砾砂岩;8—上三叠统页岩、砂岩、粉砂岩;9—中下二叠统灰岩、泥灰岩;10—巴特斯阶砾岩、砂岩和页岩;11—下白垩统砂岩、页岩;12—晚中生代辉长岩;13—第四系;14—产状;15—断层;16—采样位置

Fig. 1 Simplified geological map of the Murgab area, southeast Pamir (modified after Geological Map of Soviet Union at the scale of 1:200 000 published in 1967)

1—Schist and marble of Sarjil Formation; 2—Shale, sandstone and limestone of Kulakeli Formation; 3—Limestone, sandstone and volcanic rocks of Lower Silurian; 4—Limestone and shale of Upper Silurian; 5—Limestone of Lower Devonian; 6—Limestone and dolomite of Middle Devonian; 7—Limestone and pebbly sandstone of Upper Carboniferous to Permian; 8—Shale, sandstone and siltstone of Upper Triassic; 9—Limestone and marlstone of Middle-Lower Permian; 10—Conglomerate, sandstone and shale of Butters Stage; 11—Sandstone and shale of Lower Cretaceous; 12—Late Mesozoic gabbro; 13—Quaternary; 14—Attitude; 15—Fault; 16—Sampling location

密切共生,从野外关系判断,两者存在相互穿插关系,为近同期侵入(图2b)。该侵入岩带位于中、南帕米尔地体交界Rushan-Pshart缝合带中。岩体呈岩株、岩枝状产出,主要沿穆尔尕布断裂以北分布,侵入晚元古代(?)萨尔吉尔加组中,围岩主要为浅变质碎屑岩。

岩体露头较好,总体较为新鲜,主要岩性为辉长岩,部分岩体由辉长岩和闪长岩组成。辉长岩呈深灰-灰黑色,中粗粒结构,主要组成包括斜长石(40%~45%)、辉石(35%~40%)和角闪石(5%~10%),常见副矿物包括榍石、磷灰石、锆石和金属矿物磁铁矿。在镜下观察,辉长岩具有典型的辉长结构,矿物颗粒一般为1~4 mm。其中,可见单斜辉石

和斜方辉石两类辉石(图2c),多呈自形-半自形粒状,与斜长石镶嵌分布,自形程度相近,部分辉石边缘发生次闪石化(图2d),斜长石多为板条状,发育卡钠复合双晶(图2e);闪长岩类,呈浅灰-灰色,半自形中细粒粒状结构,主要由斜长石(60%~65%)和角闪石(20%~25%)、石英(5%)和少量黑云母组成,黑云母呈半自形叶片状,粒径0.2~0.5 mm,其中包含针状金红石,黑云母多发生绿泥石化,少量退变为白云母(图2f)。

3 样品及分析方法

在穆尔尕布北侧三处基性岩体中采集辉长岩和闪长岩样品共13件。样品的主量元素、微量和稀

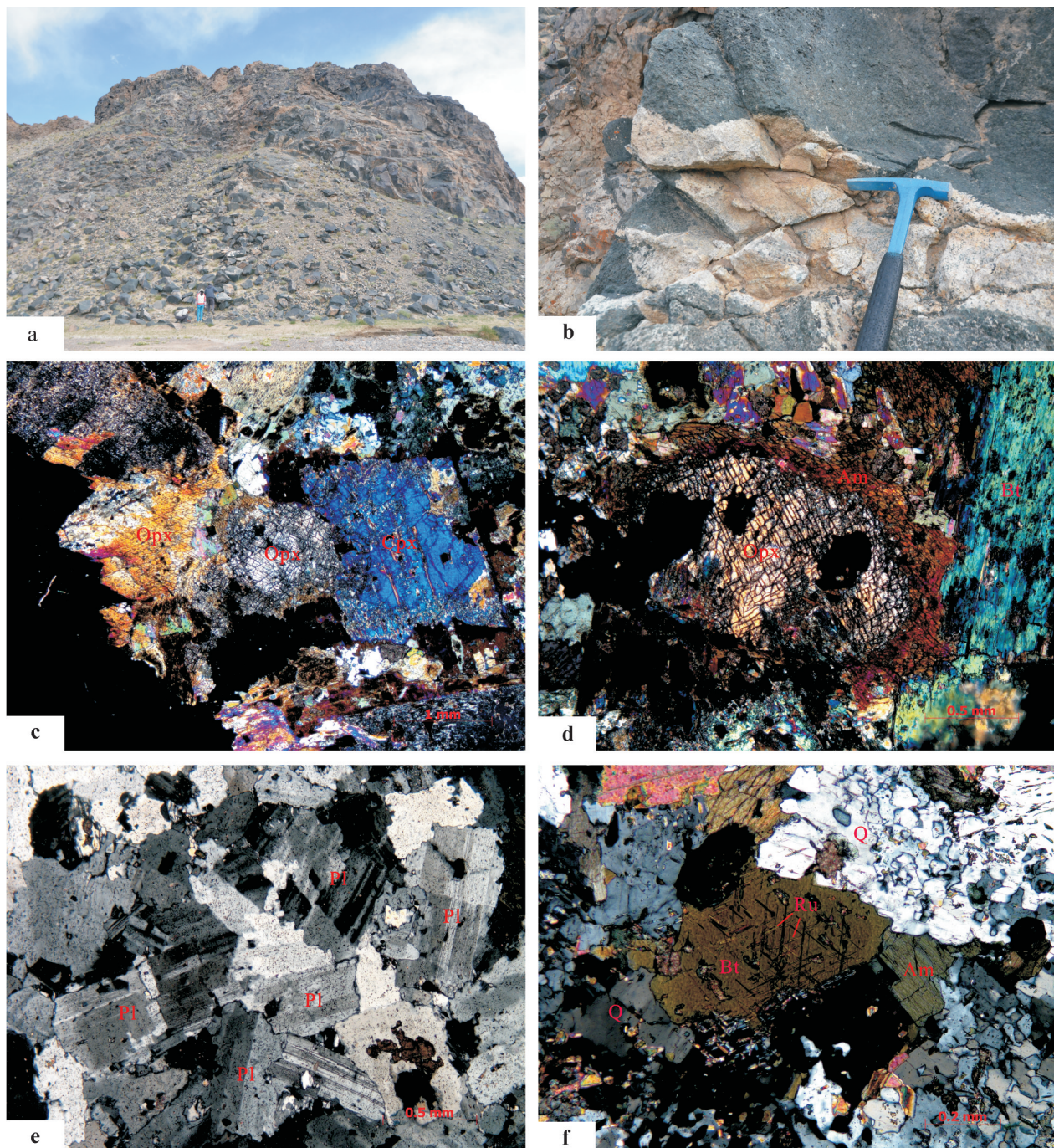


图2 穆尔尕布辉长岩-闪长岩野外及镜下照片

a—穆尔尕布杂岩体野外宏观照片;b—浅色细粒闪长质脉体穿插深灰色辉长岩中;c—辉长岩中的单斜辉石和斜方辉石晶体(正交偏光);d—单斜辉石边部蚀变为角闪石,核部仍保留(正交偏光);e—闪长岩中长石的卡纳复合双晶(正交偏光);f—辉长岩中发现呈针状的金红石(正交偏光);Opx—斜方辉石;Cpx—单斜辉石;Am—角闪石;Bt—黑云母;Pl—斜长石;Ru—金红石;Q—石英

Fig.2 Macroscopic and microscopic photographs of Murgab gabbro and diorite

a—Field macroscopic photograph of Murgab complex; b—The light color diorite dyke intruded into dark grey gabbro; c—Orthopyroxene and clinopyroxene in the gabbro(cross-polarized light); d—The edge of clinopyroxene has been altered to amphibole, the core is unaltered (cross-polarized light);e—Carlsbad-albite compound twin feldspar in diorite(cross-polarized light); f—Needle-like rutile in gabbro (cross-polarized light); Opx—Orthopyroxene; Cpx—Clinopyroxene; Am—Amphibole; Bt—Biotite; Pl—Plagioclase; Ru—Rutile; Q—Quartz

土元素在中国地质调查局西安地质调查中心实验测试中心分析完成。主量元素采用X-荧光光谱仪测定,仪器编号SX-45,分析误差低于2%;微量元素和稀土元素利用电感耦合等离子体-质谱ICP-MS仪器分析完成,分析误差优于5%~10%;检测依据为GB/T14506.2/14/28-2010和DZ/T0223-2001。

辉长岩和闪长岩的锆石分选在河北省区域地质调查队实验室完成,采用常规重力和电磁分选方法,然后在双目镜下手工挑纯,选出晶形较好、无裂隙,具代表性的锆石粘在双面胶上,用无色透明的环氧树脂固定,待环氧树脂充分固化后抛光,进行透射光、反射光和阴极发光(CL)扫描电镜显微照相。根据反射光、透射光及锆石阴极发光图像的分析,选择吸收程度较为均匀的区域进行U-Pb测年和Hf同位素分析。阴极发光照相和锆石U-Pb测年及微量元素分析在中国地质调查局西安地质调查中心实验测试中心利用激光剥蚀-电感耦合等离子体质谱(LA-ICP-MS)同时完成。实验室所采用的激光束斑直径为32 μm,剥蚀深度20~40 μm,激光脉冲8 Hz,锆石年龄测试采用标准锆石91500作为外部标准物质,元素含量采用NIST610作为外标,²⁹Si作为内标元素。详细测试流程、方法质量监控步骤等见文献(Horn et al., 2000; Ballard et al., 2001; Kosler et al., 2002; Yuan et al., 2004)。锆石的同位素比值及元素含量计算采用Glitter (ver4.0, Macquarie University)软件,采用Isoplot 3(2006)程序进行锆石U-Pb年龄加权平均值计算及谐和图的绘制(Ludwig, 2003)。

锆石原位Lu-Hf同位素分析在西北大学大陆动力学重点实验室利用Nu Plasma型MC-ICP-MS完成,激光剥蚀系统为配备有193 nm ArF准分子激光器的GeoLas2005。在已测过年龄的锆石颗粒上选择相同或相近的区域进行Hf同位素测试,激光束斑直径44 μm,剥蚀频率为10Hz,具体分析方法和仪器参数详见Yuan et al., (2008)。样品测定过程中以标准锆石91500为标样,并同时测定标准锆石GJ-1。 ε_{Hf} 计算采用¹⁷⁶Lu衰变常数为 $1.865 \times 10^{-11} \text{ a}^{-1}$ (Scherer et al., 2001),球粒陨石现今值¹⁷⁶Hf/¹⁷⁷Hf=0.282772和¹⁷⁶Lu/¹⁷⁷Hf=0.0332(Blichert and Albarede, 1997),单阶段亏损地幔Hf模式年龄(T_{DM1})计算采用现今亏损地幔值¹⁷⁶Hf/¹⁷⁷Hf=0.282772和¹⁷⁶Lu/¹⁷⁷Hf=0.0384(Griffin et al., 2000)。

4 分析结果

4.1 主量元素特征

分析结果(表1)显示,穆尔尕布辉长岩SiO₂含量较低,为46.5%~49.94%,TiO₂为1.84%~3.31%,Al₂O₃为1.84%~3.31%,MgO含量较高,为9.01%~15.67%,Mg[#]值为63.62~72.68,ALK(K₂O+Na₂O)介于2.49%~4.99%。在SiO₂-K₂O图解(图3a)上,辉长岩样品点均落入低钾(拉斑)系列;在岩石TAS图解(图3b)上,样品基本落入亚碱性系列的辉长岩区域。

闪长岩类:其地球化学组成显示富Si、Al,贫Mg、低Ti的特征,SiO₂含量为52.53%~62.55%,Al₂O₃为16.3%~18.29%,MgO含量0.91%~1.31%,Mg[#]值变化较大,为39.22~58.92,TiO₂为0.94%~1.69%;全碱含量相对较高,ALK(K₂O+Na₂O)为7.81%~10.23%,Na₂O/K₂O为11.16~23.56,明显富钠贫钾。在SiO₂-K₂O图解(图3a)上,闪长岩类样品点落入钙碱性-高钾钙碱性系列;在SiO₂-(Na₂O+K₂O)图解(图3b)上,样品点落入碱性系列二长岩、正长岩区域。

4.2 稀土及微量元素特征

穆尔尕布辉长岩和闪长岩的稀土元素球粒陨石标准化配分型式均呈轻稀土富集型(图4a),轻、重稀土显示一定程度的分馏,稀土元素总量较高,ΣREE=167.18×10⁻⁶~385.92×10⁻⁶,轻、重稀土比值ΣLREE/ΣHREE=7.05~16.22,(La/Yb)_N=11.19~27.41。闪长岩类轻、重稀土分流程度更高,其δEu=1.19~1.97,δCe=0.96~1.03,显示Eu和Ce基本无亏损,辉长岩的δEu=0.85~0.99,δCe=0.96~1.03。可见辉长岩和闪长岩均无明显Ce异常,但前者无明显Eu异常,而后者显示轻微正Eu异常。

样品的微量元素分析结果见表1,辉长岩和闪长岩类微量元素原始地幔标准化蛛网图(图4b)显示,两者整体上具有相似的标准化曲线形式,表现为重稀土配分曲线相对平坦,轻稀土相对富集,Rb、Ba、Th、U等大离子亲石元素(LILE)明显富集,高场强元素(HFES)中P和Ti显著亏损,而Nb、Ta含量则相对较高,显示K、Sr、P和Ti元素明显的负异常,Sr的负异常指示岩浆发生斜长石的分异作用,P和Ti含量偏低可能与磷灰石、钛铁矿或金红石的结晶分异有关。

4.3 锆石U-Pb年龄及Hf同位素

该岩体侵入地层为新元古代(或古生代)弱变

表1 帕米尔地区穆尔尕布基性杂岩体主量元素(%)、微量元素(10⁻⁶)和稀土元素(10⁻⁶)分析结果
Table 1 Abundances of major elements (%), trace elements and rare earth elements (10⁻⁶) of the Murgub mafic complex in Pamir area

| 样品编号 | M810-1 | M810-2 | M810-3 | M810-4 | M810-5 | M810-6 | M810-7 | M810-8 | M810-9 | M810-10 | M810-11 | M810-12 | M810-13 | |
|------------------------------------|--------|--------|--------|--------|--------|--------|--------|--------|--------|---------|---------|---------|---------|-----|
| 样品名称 | 闪长岩 | 闪长岩 | 闪长岩 | 闪长岩 | 闪长岩 |
| SiO ₂ | 62.55 | 61.69 | 62.62 | 62.12 | 61.35 | 56.69 | 52.53 | 47.56 | 47.28 | 49.94 | 47.03 | 46.5 | 48.79 | |
| TiO ₂ | 0.94 | 1.00 | 0.97 | 0.99 | 1.05 | 1.69 | 2.38 | 2.8 | 2.85 | 2.66 | 2.25 | 3.31 | 1.84 | |
| Al ₂ O ₃ | 18.28 | 18.50 | 18.65 | 18.72 | 18.29 | 18.41 | 16.3 | 8.74 | 8.85 | 11.3 | 7.28 | 7.2 | 6.72 | |
| Fe ₂ O ₃ | 1.24 | 0.99 | 0.72 | 1.39 | 1.67 | 2.80 | 3 | 3.99 | 3.8 | 3.48 | 3.86 | 4.03 | 3.92 | |
| FeO | 1.02 | 1.16 | 1.00 | 1.12 | 1.34 | 2.23 | 3.55 | 7.28 | 7.04 | 6.05 | 6.92 | 7.27 | 7.17 | |
| MnO | 0.03 | 0.04 | 0.02 | 0.02 | 0.03 | 0.03 | 0.05 | 0.11 | 0.11 | 0.09 | 0.11 | 0.12 | 0.11 | |
| MgO | 0.91 | 1.31 | 1.08 | 0.98 | 1.31 | 1.72 | 5.03 | 12.52 | 11.76 | 9.01 | 15.52 | 13.57 | 15.67 | |
| CaO | 3.23 | 3.58 | 2.93 | 2.76 | 3.56 | 6.10 | 6.97 | 11.7 | 12.83 | 10.22 | 11.87 | 13.34 | 11.16 | |
| Na ₂ O | 9.66 | 9.19 | 9.44 | 9.37 | 9.04 | 8.31 | 6.47 | 2.2 | 1.94 | 4.15 | 1.48 | 1.47 | 1.58 | |
| K ₂ O | 0.41 | 0.65 | 0.79 | 0.70 | 0.81 | 0.55 | 1.34 | 1.06 | 1.24 | 0.84 | 1.3 | 1.02 | 0.99 | |
| P ₂ O ₅ | 0.14 | 0.17 | 0.13 | 0.14 | 0.15 | 0.28 | 0.43 | 0.29 | 0.28 | 0.28 | 0.27 | 0.26 | 0.05 | |
| LOI | 0.44 | 0.45 | 0.34 | 0.37 | 1.08 | 0.49 | 0.8 | 0.5 | 0.43 | 0.4 | 0.36 | 0.39 | 0.51 | |
| Total | 98.85 | 98.73 | 98.69 | 98.68 | 99.68 | 99.30 | 98.85 | 98.75 | 98.41 | 98.42 | 98.25 | 98.48 | 98.51 | |
| Na ₂ O/K ₂ O | 23.56 | 14.14 | 11.95 | 13.39 | 11.16 | 15.11 | 4.83 | 2.08 | 1.56 | 4.94 | 1.14 | 1.44 | 1.60 | |
| Mg [#] | 43.15 | 53.23 | 53.87 | 42.41 | 45.09 | 39.22 | 58.92 | 67.24 | 66.70 | 63.62 | 72.68 | 68.93 | 72.30 | |
| Li | 10.5 | 12.1 | 14.4 | 13.8 | 16.6 | 16.1 | 21.1 | 21.6 | 23.6 | 15.7 | 18.0 | 18.4 | 16.8 | |
| Be | 2.00 | 2.13 | 1.29 | 1.59 | 1.65 | 3.64 | 1.52 | 1.56 | 1.23 | 1.49 | 1.14 | 1.86 | | |
| Sc | 9.14 | 6.11 | 4.98 | 6.09 | 4.17 | 8.22 | 10.8 | 30.7 | 35.2 | 29.2 | 56.2 | 49.8 | 39.5 | |
| V | 48.2 | 41.8 | 35.3 | 32.4 | 40.2 | 69.2 | 128 | 286 | 280 | 277 | 234 | 299 | 186 | |
| Cr | 14.4 | 20.8 | 10.5 | 14.3 | 27.0 | 13.7 | 109 | 822 | 808 | 307 | 1180 | 986 | 1100 | |
| Co | 3.10 | 6.99 | 3.32 | 3.92 | 6.56 | 9.10 | 24.7 | 51.9 | 44.2 | 42.6 | 61.4 | 56.4 | 65.4 | |
| Ni | 23.1 | 38.1 | 19.7 | 20.0 | 22.3 | 10.4 | 127 | 213 | 155 | 190 | 304 | 240 | 264 | |
| Cu | 13.0 | 13.2 | 9.40 | 13.0 | 14.8 | 16.4 | 25.6 | 29.8 | 34.2 | 52.1 | 32.9 | 49.5 | 38.2 | |
| Zn | 27.1 | 5.65 | 12.7 | 1.98 | 36.3 | 13.2 | 31.3 | 59.6 | 62.4 | 29.8 | 42.6 | 72.9 | 55.4 | |
| Ga | 23.6 | 24.1 | 20.5 | 20.7 | 20.4 | 23.8 | 20.6 | 16.5 | 17.0 | 17.8 | 14.3 | 14.5 | 15.2 | |
| Rb | 17.2 | 18.3 | 23.0 | 12.6 | 23.6 | 8.94 | 35.7 | 27.8 | 33.4 | 18.0 | 33.9 | 22.4 | 40.1 | |
| Sr | 455 | 472 | 366 | 490 | 430 | 1050 | 873 | 349 | 425 | 236 | 117 | 194 | 63.9 | |
| Ba | 346 | 255 | 251 | 508 | 538 | 215 | 774 | 278 | 378 | 171 | 382 | 231 | 133 | |
| Zr | 42.3 | 46.4 | 54.0 | 49.3 | 41.1 | 104 | 34.7 | 76.6 | 64.4 | 73.4 | 83.6 | 78.2 | 26.6 | |

续表1

| 样品编号 | M810-1 | M810-2 | M810-3 | M810-4 | M810-5 | M810-6 | M810-7 | M810-8 | M810-9 | M810-10 | M810-11 | M810-12 | M810-13 | |
|-----------------------------------|--------|--------|--------|--------|--------|--------|--------|--------|--------|---------|---------|---------|---------|--------|
| 样品名称 | 闪长岩 | 闪长岩 | 闪长岩 | 闪长岩 | 闪长岩 |
| Hf | 2.07 | 1.39 | 2.03 | 1.76 | 4.65 | 1.60 | 3.79 | 3.45 | 3.41 | 3.84 | 3.90 | 3.84 | 3.90 | 1.83 |
| Nb | 124 | 88.5 | 85.9 | 81.1 | 86.4 | 144 | 102 | 48.2 | 46.8 | 37.7 | 41.8 | 43.0 | 43.0 | 74.2 |
| Ta | 8.33 | 6.08 | 6.88 | 6.01 | 6.29 | 10.2 | 7.55 | 3.72 | 3.52 | 2.82 | 3.12 | 3.37 | 3.37 | 5.52 |
| Mo | 0.64 | 0.52 | 0.58 | 0.90 | 1.67 | 0.43 | 0.47 | 1.02 | 0.70 | 1.84 | 0.80 | 0.91 | 0.80 | 0.45 |
| Cs | 0.68 | 0.77 | 1.26 | 0.89 | 1.30 | 0.99 | 2.64 | 1.24 | 1.06 | 1.24 | 1.86 | 0.66 | 0.66 | 5.01 |
| La | 74.9 | 55.0 | 66.5 | 40.2 | 53.8 | 101 | 76.2 | 44.4 | 36.2 | 30.1 | 24.5 | 29.4 | 29.4 | 52.1 |
| Ce | 170 | 108 | 132 | 83.9 | 110 | 209 | 159 | 93.4 | 80.0 | 65.2 | 59.6 | 67.2 | 67.2 | 98.5 |
| Pr | 21.2 | 12.7 | 15.1 | 9.72 | 12.7 | 24.8 | 18.9 | 11.7 | 10.2 | 8.31 | 8.22 | 8.87 | 8.87 | 11.1 |
| Nd | 77.5 | 46.6 | 54.3 | 36.1 | 46.3 | 91.3 | 72.5 | 44.2 | 41.0 | 33.8 | 34.2 | 34.2 | 34.2 | 41.0 |
| Srn | 12.2 | 7.45 | 8.65 | 5.75 | 7.44 | 14.8 | 12.4 | 9.06 | 8.68 | 7.88 | 7.40 | 7.71 | 7.71 | 8.21 |
| Eu | 4.29 | 2.80 | 4.23 | 3.36 | 3.95 | 5.02 | 4.78 | 2.79 | 2.48 | 2.49 | 2.17 | 2.22 | 2.22 | 2.12 |
| Gd | 9.21 | 6.08 | 6.63 | 4.38 | 5.51 | 11.4 | 9.48 | 7.71 | 7.30 | 7.36 | 6.30 | 6.66 | 6.66 | 6.71 |
| Tb | 1.35 | 0.89 | 0.93 | 0.65 | 0.82 | 1.64 | 1.34 | 1.10 | 1.04 | 1.12 | 0.92 | 0.95 | 0.95 | 1.03 |
| Dy | 6.99 | 4.44 | 4.56 | 3.26 | 3.86 | 7.87 | 6.54 | 5.64 | 5.48 | 6.22 | 4.60 | 4.99 | 4.99 | 5.31 |
| Ho | 1.29 | 0.80 | 0.79 | 0.59 | 0.68 | 1.47 | 1.15 | 0.99 | 0.94 | 1.10 | 0.80 | 0.85 | 0.85 | 0.92 |
| Er | 3.33 | 2.19 | 2.13 | 1.50 | 1.93 | 3.61 | 2.81 | 2.45 | 2.34 | 2.63 | 1.90 | 2.07 | 2.07 | 2.43 |
| Tm | 0.48 | 0.30 | 0.29 | 0.22 | 0.28 | 0.47 | 0.38 | 0.32 | 0.31 | 0.36 | 0.25 | 0.28 | 0.28 | 0.35 |
| Yb | 2.81 | 1.87 | 1.74 | 1.34 | 1.75 | 2.69 | 2.14 | 1.77 | 1.75 | 1.93 | 1.43 | 1.57 | 1.57 | 2.09 |
| Lu | 0.37 | 0.27 | 0.24 | 0.20 | 0.26 | 0.37 | 0.29 | 0.24 | 0.23 | 0.25 | 0.21 | 0.21 | 0.21 | 0.29 |
| Y | 27.6 | 19.0 | 16.7 | 11.4 | 15.4 | 29.6 | 23.3 | 20.7 | 20.2 | 22.8 | 17.4 | 17.9 | 17.9 | 21.1 |
| Pb | 4.92 | 5.93 | 4.00 | 4.31 | 6.54 | 3.58 | 8.05 | 7.00 | 14.8 | 1.90 | 6.17 | 6.85 | 6.85 | 7.23 |
| Th | 11.4 | 15.6 | 6.52 | 4.24 | 6.43 | 9.02 | 3.49 | 3.52 | 3.38 | 2.30 | 4.30 | 3.10 | 3.10 | 10.2 |
| U | 1.68 | 1.63 | 1.91 | 1.59 | 1.76 | 2.33 | 1.73 | 1.30 | 0.90 | 0.97 | 0.97 | 0.71 | 0.71 | 1.12 |
| ΣREE | 385.92 | 249.39 | 298.09 | 191.17 | 249.28 | 475.44 | 367.91 | 225.77 | 197.95 | 168.75 | 152.50 | 167.18 | 167.18 | 232.16 |
| LREE | 360.09 | 232.55 | 280.78 | 179.03 | 234.19 | 445.92 | 343.78 | 205.55 | 178.56 | 147.78 | 136.09 | 149.60 | 149.60 | 213.03 |
| HREE | 25.83 | 16.84 | 17.31 | 12.14 | 15.09 | 29.52 | 24.13 | 20.22 | 19.39 | 20.97 | 16.41 | 17.58 | 17.58 | 19.13 |
| LREE/HREE (La/Yb) _N | 13.94 | 13.81 | 16.22 | 14.75 | 15.52 | 15.11 | 14.25 | 10.17 | 9.21 | 7.05 | 8.29 | 8.51 | 8.51 | 11.14 |
| δ Eu | 1.19 | 1.23 | 1.64 | 1.97 | 1.81 | 1.14 | 1.30 | 0.99 | 0.93 | 0.98 | 0.95 | 0.92 | 0.92 | 0.85 |
| δ Ce | 1.03 | 0.96 | 0.98 | 1.01 | 1.00 | 0.99 | 1.00 | 0.98 | 1.01 | 0.99 | 1.03 | 1.01 | 1.01 | 0.96 |

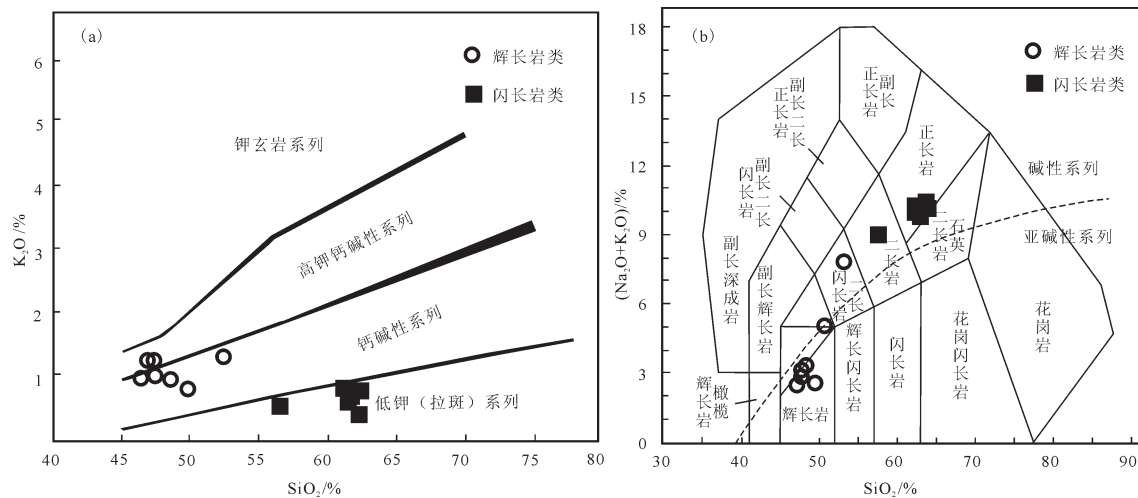


图3 穆尔尕布辉长岩-闪长岩 SiO_2 - K_2O 图解(a)和 SiO_2 - $(\text{Na}_2\text{O}+\text{K}_2\text{O})$ 图解(b)
 Fig.3 SiO_2 - K_2O diagram (a) and SiO_2 - $(\text{Na}_2\text{O}+\text{K}_2\text{O})$ diagram (b) of Murgab gabbro and diorite

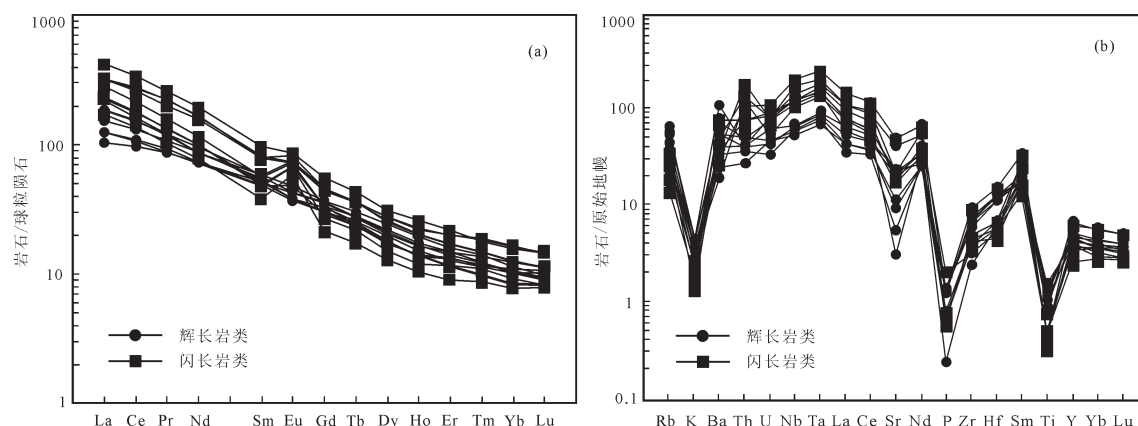


图4 穆尔尕布辉长岩-闪长岩稀土元素球粒陨石标准化配分型式图(a)及微量元素原始地幔标准化蛛网图(b)(球粒陨石标准值、原始地幔标准值据 Sun et al., 1989)

Fig. 4 Chondrite-normalized REE patterns (a) and primitive mantle (PM)-normalized spider diagram (b) of Murgab gabbro and diorite

质碎屑岩中,岩石较为新鲜,未发生明显的变形和变质作用。本次在辉长岩和闪长岩中采集同位素年龄样品各1件开展锆石LA-ICP-MS U-Pb年代学研究。

两类岩石中锆石多为浅黄色、自形-半自形短柱状颗粒,晶形相对完整,部分为不完整晶体,长度一般在80~200 μm。阴极发光(CL)图像是揭示锆石内部结构的有效手段(Vavra et al.,1996; 吴元保等,2004),对锆石内部结构分析是合理解释测年的重要依据。所测试样品的锆石阴极发光图像(图5)显示,大部分锆石具有明显的震荡环带且环带较宽,闪长岩中部分锆石显示似核边结构,辉长岩中

少量锆石为弱震荡环带或板状结构,属于岩浆结晶锆石(吴元保等,2004)。利用LA-ICP-MS对闪长岩MS和辉长岩MH中锆石分别进行了U-Pb年龄和微量元素测定,获得的同位素比值及年龄结果见表2。其Th和U含量变化范围较大,但Th/U比值在0.56~2.35,大部分集中在1.0左右,也显示出岩浆锆石的特征(闫义等,2003)。

锆石 U-Pb 谐和图(图 6)显示,闪长岩中 27 个分析点均位于谐和线上或其附近,其 $^{206}\text{Pb}/^{238}\text{U}$ 年龄非常集中,锆石边部和核部测得的年龄结果相近,在 222~239 Ma,其年龄加权平均值为 $(231.5 \pm 1.9)\text{ Ma}$ ($\text{MSWD}=1.4$)(图 6)。辉长岩中 28 个分析点全部落

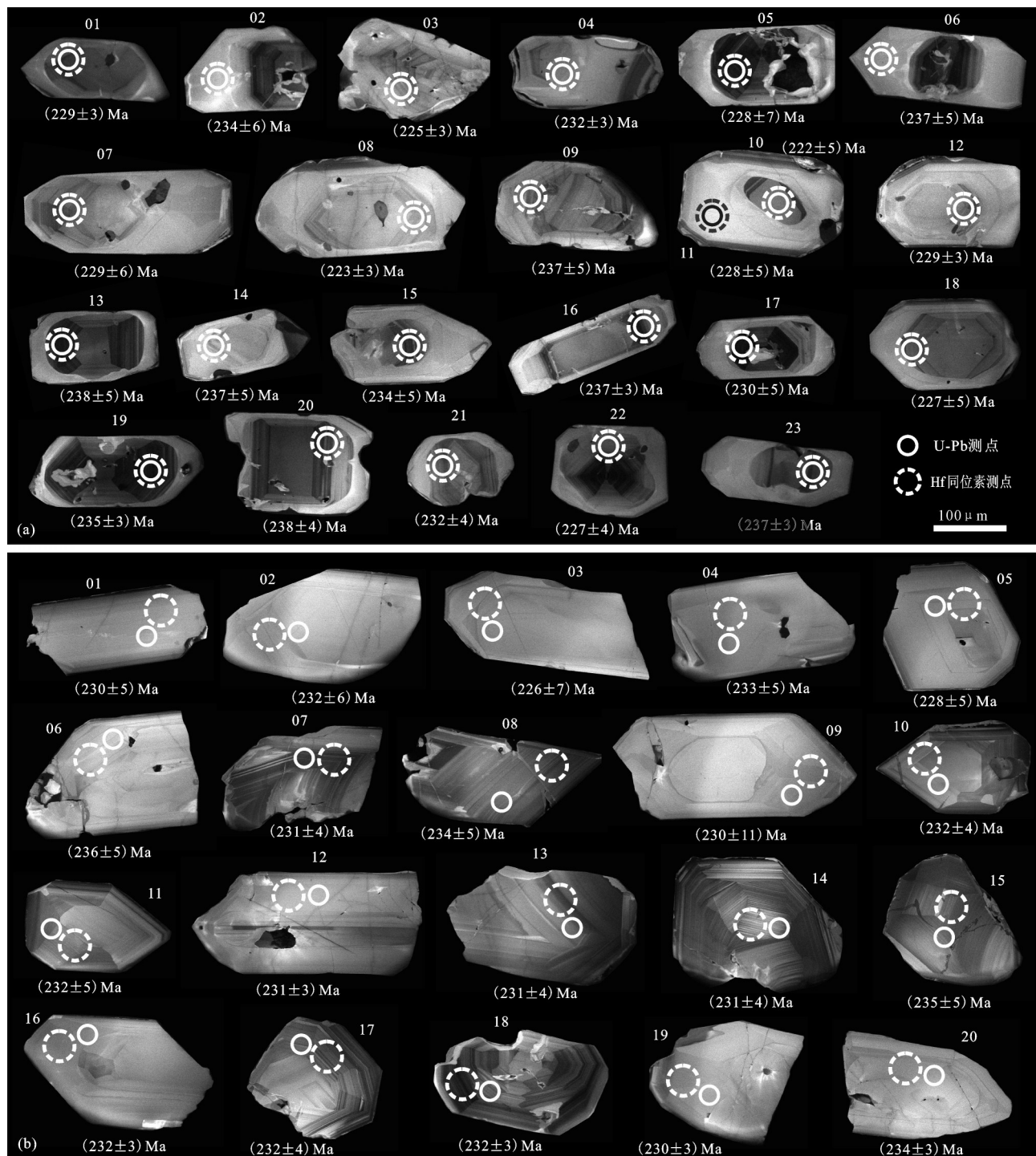


图5 帕米尔地区穆尔尕布中基性杂岩体的锆石阴极发光CL图像 a—闪长岩; b—辉长岩

Fig. 5 Representative CL images of zircons from Murgab mafic complex, Pamira-Diorite; b—Gabbro

表2 穆尔尕布辉长-闪长岩中锆石LA-ICP-MS U-Pb分析结果
Table 2 LA-ICP-MS zircon U-Pb dating results of Murgab gabbro and diorite

| 分析号 | Th | U | Th/U | 同位素比值 | | | | | | 年龄 / Ma | | | | | |
|-------|-----------|--------|------|-----------------------------------|-----------|----------------------------------|-----------|----------------------------------|-----------|-----------------------------------|-----------|----------------------------------|-----------|----------------------------------|-----------|
| | 10^{-6} | 10^6 | | $^{207}\text{Pb}/^{206}\text{Pb}$ | 1σ | $^{207}\text{Pb}/^{235}\text{U}$ | 1σ | $^{206}\text{Pb}/^{238}\text{U}$ | 1σ | $^{207}\text{Pb}/^{206}\text{Pb}$ | 1σ | $^{207}\text{Pb}/^{235}\text{U}$ | 1σ | $^{206}\text{Pb}/^{238}\text{U}$ | 1σ |
| MS-01 | 2547 | 1292 | 1.97 | 0.05298 | 0.0021 | 0.2645 | 0.0074 | 0.03621 | 0.0005 | 328 | 88 | 238 | 6 | 229 | 3 |
| MS-02 | 28 | 36 | 0.77 | 0.05161 | 0.0066 | 0.2625 | 0.0322 | 0.0369 | 0.0009 | 268 | 267 | 237 | 26 | 234 | 6 |
| MS-03 | 783 | 489 | 1.60 | 0.04979 | 0.0023 | 0.2440 | 0.0086 | 0.03554 | 0.0005 | 185 | 103 | 222 | 7 | 225 | 3 |
| MS-04 | 1106 | 733 | 1.51 | 0.04999 | 0.0019 | 0.2522 | 0.0061 | 0.03658 | 0.0005 | 195 | 84 | 228 | 5 | 232 | 3 |
| MS-05 | 27 | 35 | 0.76 | 0.05237 | 0.0080 | 0.2600 | 0.0384 | 0.036 | 0.0012 | 302 | 315 | 235 | 31 | 228 | 7 |
| MS-06 | 38 | 50 | 0.76 | 0.05096 | 0.0053 | 0.2628 | 0.0259 | 0.0374 | 0.0008 | 239 | 222 | 237 | 21 | 237 | 5 |
| MS-07 | 40 | 46 | 0.87 | 0.05605 | 0.0074 | 0.2791 | 0.0352 | 0.03612 | 0.0010 | 454 | 268 | 250 | 28 | 229 | 6 |
| MS-08 | 2439 | 1229 | 1.98 | 0.0514 | 0.0018 | 0.2497 | 0.0054 | 0.03523 | 0.0005 | 259 | 80 | 226 | 4 | 223 | 3 |
| MS-09 | 112 | 78 | 1.43 | 0.05113 | 0.0056 | 0.2641 | 0.0273 | 0.03746 | 0.0009 | 247 | 232 | 238 | 22 | 237 | 5 |
| MS-10 | 356 | 202 | 1.76 | 0.05471 | 0.0046 | 0.2648 | 0.0203 | 0.0351 | 0.0008 | 400 | 177 | 239 | 16 | 222 | 5 |
| MS-11 | 82 | 96 | 0.86 | 0.0545 | 0.0050 | 0.2709 | 0.0231 | 0.03605 | 0.0008 | 392 | 193 | 243 | 18 | 228 | 5 |
| MS-12 | 1268 | 800 | 1.59 | 0.05114 | 0.0019 | 0.2547 | 0.0064 | 0.03612 | 0.0005 | 247 | 85 | 230 | 5 | 229 | 3 |
| MS-13 | 43 | 59 | 0.74 | 0.04674 | 0.0049 | 0.2424 | 0.0242 | 0.03761 | 0.0008 | 36 | 233 | 220 | 20 | 238 | 5 |
| MS-14 | 80 | 89 | 0.90 | 0.05126 | 0.0041 | 0.2644 | 0.0194 | 0.0374 | 0.0008 | 253 | 173 | 238 | 16 | 237 | 5 |
| MS-15 | 53 | 96 | 0.56 | 0.05202 | 0.0054 | 0.2651 | 0.0259 | 0.03696 | 0.0008 | 286 | 219 | 239 | 21 | 234 | 5 |
| MS-16 | 1250 | 820 | 1.53 | 0.05174 | 0.0021 | 0.2676 | 0.0077 | 0.03752 | 0.0005 | 274 | 90 | 241 | 6 | 237 | 3 |
| MS-17 | 52 | 69 | 0.76 | 0.05223 | 0.0045 | 0.2618 | 0.0207 | 0.03636 | 0.0008 | 296 | 183 | 236 | 17 | 230 | 5 |
| MS-18 | 439 | 253 | 1.73 | 0.0552 | 0.0041 | 0.2728 | 0.0182 | 0.03585 | 0.0007 | 420 | 157 | 245 | 15 | 227 | 5 |
| MS-19 | 668 | 284 | 2.35 | 0.05003 | 0.0023 | 0.2558 | 0.0093 | 0.03708 | 0.0006 | 196 | 105 | 231 | 8 | 235 | 3 |
| MS-20 | 142 | 134 | 1.06 | 0.05177 | 0.0032 | 0.2678 | 0.0143 | 0.03753 | 0.0006 | 275 | 134 | 241 | 11 | 238 | 4 |
| MS-21 | 93 | 89 | 1.04 | 0.0516 | 0.0040 | 0.2606 | 0.0184 | 0.03663 | 0.0007 | 268 | 167 | 235 | 15 | 232 | 4 |
| MS-22 | 361 | 301 | 1.20 | 0.05189 | 0.0029 | 0.2566 | 0.0124 | 0.03586 | 0.0006 | 280 | 125 | 232 | 10 | 227 | 4 |
| MS-23 | 320 | 250 | 1.28 | 0.05037 | 0.0023 | 0.2605 | 0.0091 | 0.03751 | 0.0006 | 212 | 101 | 235 | 7 | 237 | 3 |
| MS-24 | 23 | 32 | 0.73 | 0.04832 | 0.0071 | 0.2520 | 0.0360 | 0.03783 | 0.0010 | 115 | 314 | 228 | 29 | 239 | 6 |
| MS-25 | 139 | 111 | 1.26 | 0.05131 | 0.0040 | 0.2568 | 0.0185 | 0.03631 | 0.0007 | 255 | 171 | 232 | 15 | 230 | 4 |
| MS-26 | 129 | 139 | 0.93 | 0.05079 | 0.0032 | 0.2569 | 0.0142 | 0.03668 | 0.0006 | 232 | 139 | 232 | 11 | 232 | 4 |
| MS-27 | 235 | 170 | 1.38 | 0.05154 | 0.0032 | 0.2650 | 0.0142 | 0.0373 | 0.0007 | 265 | 135 | 239 | 11 | 236 | 4 |
| MH-01 | 111 | 86 | 1.30 | 0.04878 | 0.0044 | 0.2444 | 0.0208 | 0.03634 | 0.0007 | 137 | 200 | 222 | 17 | 230 | 5 |
| MH-02 | 135 | 94 | 1.44 | 0.05492 | 0.0059 | 0.2771 | 0.0282 | 0.03659 | 0.0009 | 409 | 224 | 248 | 22 | 232 | 6 |
| MH-03 | 31 | 40 | 0.77 | 0.05155 | 0.0084 | 0.2541 | 0.0402 | 0.03575 | 0.0012 | 266 | 336 | 230 | 33 | 226 | 7 |
| MH-04 | 46 | 61 | 0.75 | 0.05107 | 0.0051 | 0.2587 | 0.0245 | 0.03673 | 0.0008 | 244 | 215 | 234 | 20 | 233 | 5 |
| MH-05 | 60 | 68 | 0.89 | 0.04997 | 0.0054 | 0.2478 | 0.0254 | 0.03597 | 0.0009 | 194 | 233 | 225 | 21 | 228 | 5 |
| MH-06 | 56 | 50 | 1.13 | 0.05254 | 0.0058 | 0.2698 | 0.0282 | 0.03723 | 0.0008 | 309 | 231 | 243 | 23 | 236 | 5 |
| MH-07 | 63 | 93 | 0.67 | 0.05165 | 0.0040 | 0.2599 | 0.0184 | 0.03649 | 0.0007 | 270 | 168 | 235 | 15 | 231 | 4 |
| MH-08 | 61 | 51 | 1.20 | 0.05119 | 0.0055 | 0.2608 | 0.0266 | 0.03695 | 0.0008 | 249 | 228 | 235 | 21 | 234 | 5 |
| MH-09 | 23 | 27 | 0.86 | 0.05026 | 0.0125 | 0.2520 | 0.0616 | 0.03636 | 0.0017 | 207 | 494 | 228 | 50 | 230 | 11 |
| MH-10 | 429 | 291 | 1.48 | 0.05047 | 0.0028 | 0.2548 | 0.0117 | 0.03661 | 0.0006 | 217 | 122 | 230 | 10 | 232 | 4 |
| MH-11 | 140 | 99 | 1.42 | 0.05097 | 0.0041 | 0.2575 | 0.0191 | 0.03664 | 0.0007 | 239 | 175 | 233 | 15 | 232 | 5 |
| MH-12 | 611 | 416 | 1.47 | 0.04965 | 0.0028 | 0.2497 | 0.0119 | 0.03646 | 0.0006 | 179 | 126 | 226 | 10 | 231 | 4 |
| MH-13 | 416 | 353 | 1.18 | 0.05218 | 0.0024 | 0.2628 | 0.0093 | 0.03652 | 0.0006 | 293 | 101 | 237 | 7 | 231 | 3 |
| MH-14 | 320 | 236 | 1.35 | 0.05166 | 0.0026 | 0.2602 | 0.0109 | 0.03653 | 0.0006 | 271 | 113 | 235 | 9 | 231 | 4 |
| MH-15 | 85 | 85 | 1.01 | 0.05198 | 0.0052 | 0.2655 | 0.0251 | 0.03704 | 0.0008 | 285 | 213 | 239 | 20 | 235 | 5 |
| MH-16 | 427 | 466 | 0.92 | 0.05202 | 0.0023 | 0.2633 | 0.0086 | 0.0367 | 0.0005 | 286 | 96 | 237 | 7 | 232 | 3 |
| MH-17 | 118 | 159 | 0.74 | 0.05001 | 0.0031 | 0.2530 | 0.0137 | 0.03669 | 0.0006 | 195 | 138 | 229 | 11 | 232 | 4 |
| MH-18 | 320 | 360 | 0.89 | 0.05195 | 0.0025 | 0.2619 | 0.0098 | 0.03656 | 0.0006 | 283 | 105 | 236 | 8 | 232 | 3 |
| MH-19 | 837 | 732 | 1.14 | 0.04966 | 0.0019 | 0.2492 | 0.0068 | 0.03639 | 0.0005 | 179 | 89 | 226 | 5 | 230 | 3 |
| MH-20 | 347 | 340 | 1.02 | 0.05161 | 0.0024 | 0.2587 | 0.0095 | 0.03635 | 0.0006 | 268 | 103 | 234 | 8 | 230 | 3 |
| MH-21 | 828 | 645 | 1.28 | 0.0508 | 0.0020 | 0.2587 | 0.0070 | 0.03693 | 0.0005 | 232 | 88 | 234 | 6 | 234 | 3 |
| MH-22 | 805 | 472 | 1.70 | 0.05122 | 0.0022 | 0.2622 | 0.0087 | 0.03712 | 0.0006 | 251 | 98 | 237 | 7 | 235 | 3 |
| MH-23 | 291 | 248 | 1.18 | 0.05101 | 0.0026 | 0.2573 | 0.0107 | 0.03658 | 0.0006 | 241 | 113 | 233 | 9 | 232 | 4 |
| MH-24 | 63 | 54 | 1.17 | 0.05353 | 0.0084 | 0.2702 | 0.0409 | 0.0366 | 0.0013 | 351 | 320 | 243 | 33 | 232 | 8 |
| MH-25 | 148 | 129 | 1.14 | 0.05097 | 0.0034 | 0.2573 | 0.0152 | 0.03661 | 0.0007 | 239 | 146 | 233 | 12 | 232 | 4 |
| MH-26 | 857 | 528 | 1.62 | 0.05001 | 0.0021 | 0.2523 | 0.0078 | 0.03659 | 0.0005 | 195 | 94 | 229 | 6 | 232 | 3 |
| MH-27 | 95 | 96 | 0.99 | 0.05158 | 0.0043 | 0.2608 | 0.0203 | 0.03666 | 0.0007 | 267 | 181 | 235 | 16 | 232 | 4 |
| MH-28 | 162 | 212 | 0.76 | 0.04789 | 0.0026 | 0.2462 | 0.0112 | 0.03728 | 0.0006 | 93 | 124 | 224 | 9 | 236 | 4 |

在谐和线上, $^{206}\text{Pb}/^{238}\text{U}$ 年龄加权平均值为 (232.0 ± 1.5) Ma (MSWD=0.2), 代表其成岩年龄, 与闪长岩年龄近一致, 表明穆尔尕布中基性杂岩体的成岩时代为晚三叠世。

闪长岩和辉长岩样品的部分锆石 Lu-Hf 同位素分析, 结果见表 3。以 $t=232$ Ma 计算出闪长岩样品锆石 $^{176}\text{Hf}/^{177}\text{Hf}$ 初始值为 $0.282752 \sim 0.282916$, 对应的 $\epsilon_{\text{Hf}}(t)$ 为 $6.4 \sim 10.0$, 均为正值, 加权平均值为 7.9 ± 0.8 (MSWD = 2.4) (图 7a)。辉长岩样品计算结果与之相似, $\epsilon_{\text{Hf}}(t)$ 为 $4.8 \sim 12.1$, 加权平均值为 8.1 ± 1.5 (MSWD = 6.5), 表明两者母岩浆来源相同, 均来源于亏损地幔源区, 在上升过程中很少受壳源物质的污染。由于 $\epsilon_{\text{Hf}}(t)$ 均为正值, 对其进行单阶段 Hf 模 (T_{DMI}) 式年龄计算, 得到 T_{DMI} 分别为 $477 \sim 621$ Ma, $391 \sim 627$ Ma, 其加权平均值分别为 (563 ± 32) Ma (MSWD=2.3), (554 ± 58) Ma (MSWD=

5.9) (图 7b), 指示其原岩为寒武纪—前寒武纪基底。

5 讨 论

5.1 形成时代

本文对穆尔尕布岩体的高精度锆石 U-Pb 定年结果显示, 其闪长岩和辉长岩的形成时代分别是 (231.5 ± 1.9) Ma 和 (232.0 ± 1.5) Ma, 在误差范围内一致, 表明穆尔尕布中基性杂岩体的成岩时代为晚三叠世。野外观察结果表明, 在辉长岩和闪长岩的接触带附近, 见闪长岩脉体侵入辉长岩之中, 同时在闪长岩中也存在辉长岩侵入体, 指示两者近同期侵入 (图 2b), 测年结果与野外地质事实相吻合。洪俊等 (2014) 报道了南帕米尔切实界别辉长岩的年龄为 (269.5 ± 1.3) Ma, 形成时代为中二叠世早期。由于南部基性岩体在空间位置以及野外产出特征与穆

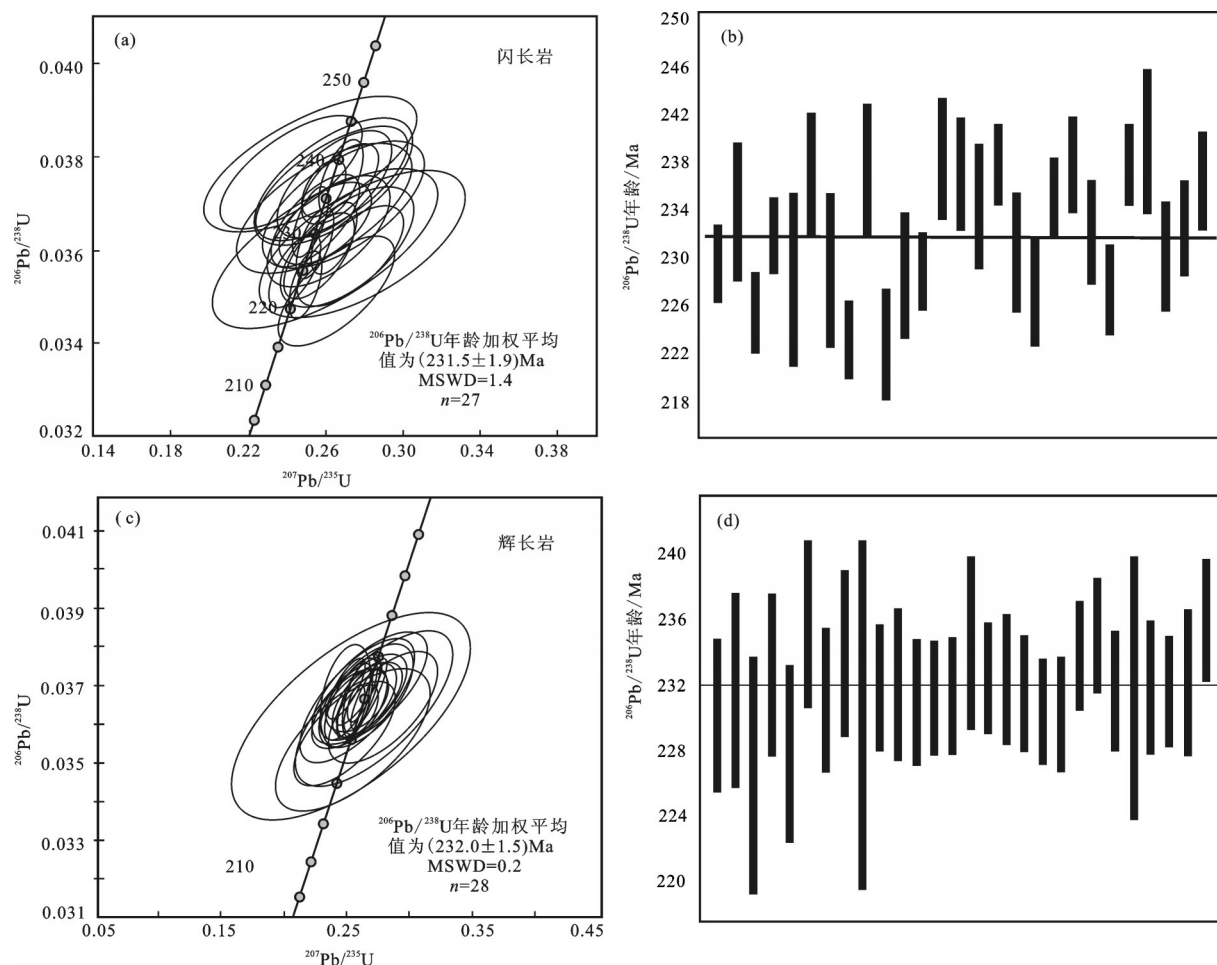


图 6 帕米尔地区穆尔尕布闪长岩和辉长岩中锆石 U-Pb 谐和图(a和c)以及 $^{206}\text{Pb}/^{238}\text{U}$ 年龄(b和d)
Fig.6 U-Pb concordia diagram (a,c) and $^{206}\text{Pb}/^{238}\text{U}$ age diagram (b, d) of zircons from diorite and gabbro of Murgab complex, Pamir

表3 帕米尔穆尔尕布辉长-闪长岩锆石 Lu-Hf 同位素组成
Table 3 Zircon Lu-Hf isotope data for gabbro and diorite of Murgab, Pamir

| 测点 | $^{176}\text{Hf}/^{177}\text{Hf}$ | 2σ | $^{176}\text{Lu}/^{177}\text{Hf}$ | $^{176}\text{Yb}/^{177}\text{Hf}$ | $\varepsilon_{\text{Hf}}(0)$ | $\varepsilon_{\text{Hf}}(t)^a$ | 1σ | T_{DM1}/Ma | 1σ | T_{DM2}/Ma | 1σ |
|-----|-----------------------------------|-----------|-----------------------------------|-----------------------------------|------------------------------|--------------------------------|-----------|----------------------------|-----------|----------------------------|-----------|
| S01 | 0.282896 | 0.000034 | 0.001175 | 0.042242 | 0.28289 | 9.3 | 1.2 | 508 | 48 | 675 | 48 |
| S02 | 0.282896 | 0.000026 | 0.001065 | 0.039327 | 0.28289 | 9.2 | 0.9 | 506 | 37 | 676 | 37 |
| S03 | 0.282860 | 0.000032 | 0.001257 | 0.047462 | 0.28285 | 8.0 | 1.1 | 559 | 45 | 755 | 45 |
| S04 | 0.282816 | 0.000025 | 0.000681 | 0.024519 | 0.28281 | 6.4 | 0.9 | 614 | 35 | 853 | 35 |
| S05 | 0.282809 | 0.000024 | 0.000569 | 0.021057 | 0.28281 | 6.4 | 0.8 | 621 | 33 | 862 | 33 |
| S06 | 0.282826 | 0.000030 | 0.000640 | 0.022407 | 0.28282 | 6.9 | 1.0 | 598 | 41 | 827 | 41 |
| S07 | 0.282885 | 0.000029 | 0.000998 | 0.037635 | 0.28288 | 9.0 | 1.0 | 521 | 41 | 697 | 41 |
| S08 | 0.282856 | 0.000030 | 0.001204 | 0.042617 | 0.28285 | 7.8 | 1.1 | 565 | 43 | 766 | 43 |
| S09 | 0.282865 | 0.000026 | 0.000763 | 0.027584 | 0.28286 | 8.3 | 0.9 | 546 | 37 | 740 | 37 |
| S10 | 0.282904 | 0.000031 | 0.000766 | 0.029433 | 0.28290 | 9.6 | 1.1 | 490 | 44 | 652 | 44 |
| S11 | 0.282854 | 0.000032 | 0.000540 | 0.020795 | 0.28285 | 7.9 | 1.1 | 557 | 45 | 763 | 45 |
| S12 | 0.282916 | 0.000030 | 0.000987 | 0.036985 | 0.28291 | 10.0 | 1.1 | 477 | 43 | 627 | 43 |
| S13 | 0.282888 | 0.000036 | 0.000786 | 0.029985 | 0.28288 | 9.1 | 1.2 | 513 | 50 | 686 | 50 |
| S14 | 0.282892 | 0.000032 | 0.001102 | 0.043751 | 0.28289 | 9.2 | 1.1 | 512 | 45 | 682 | 45 |
| S15 | 0.282908 | 0.000040 | 0.001019 | 0.039277 | 0.28290 | 9.8 | 1.4 | 488 | 56 | 645 | 56 |
| H01 | 0.282770 | 0.000026 | 0.000384 | 0.014015 | 0.28277 | 4.8 | 0.9 | 672 | 37 | 955 | 37 |
| H02 | 0.282953 | 0.000028 | 0.001218 | 0.044639 | 0.28295 | 11.3 | 1.0 | 427 | 41 | 545 | 41 |
| H03 | 0.282783 | 0.000026 | 0.000387 | 0.013434 | 0.28278 | 5.1 | 0.9 | 655 | 37 | 931 | 37 |
| H04 | 0.282810 | 0.000032 | 0.001244 | 0.050416 | 0.28281 | 6.2 | 1.1 | 631 | 46 | 870 | 46 |
| H05 | 0.282951 | 0.000033 | 0.001193 | 0.043722 | 0.28295 | 11.0 | 1.2 | 429 | 47 | 554 | 47 |
| H06 | 0.282789 | 0.000032 | 0.000588 | 0.020520 | 0.28279 | 5.5 | 1.1 | 649 | 44 | 912 | 44 |
| H07 | 0.282785 | 0.000031 | 0.000561 | 0.019175 | 0.28278 | 5.6 | 1.1 | 655 | 44 | 916 | 44 |
| H08 | 0.282978 | 0.000026 | 0.001207 | 0.048758 | 0.28297 | 12.1 | 0.9 | 391 | 37 | 489 | 37 |
| H09 | 0.282829 | 0.000029 | 0.000453 | 0.016700 | 0.28283 | 7.4 | 1.0 | 592 | 40 | 809 | 40 |
| H10 | 0.282905 | 0.000031 | 0.001026 | 0.038621 | 0.28290 | 9.8 | 1.1 | 493 | 44 | 649 | 44 |
| H11 | 0.282954 | 0.000036 | 0.001141 | 0.042145 | 0.28295 | 11.5 | 1.3 | 425 | 51 | 539 | 51 |
| H12 | 0.282842 | 0.000031 | 0.000430 | 0.015118 | 0.28284 | 7.3 | 1.1 | 572 | 44 | 795 | 44 |
| H13 | 0.282868 | 0.000030 | 0.000749 | 0.027418 | 0.28286 | 8.1 | 1.1 | 542 | 43 | 740 | 43 |
| H14 | 0.282853 | 0.000025 | 0.000896 | 0.035431 | 0.28285 | 7.9 | 0.9 | 564 | 36 | 765 | 36 |

尔尕布岩带相似,被误认为同期岩浆活动的产物。通过此次测年表明中、南帕米尔至少存在两期基性岩浆活动,分别为中二叠世和晚三叠世。

5.2 岩石成因及源区特征

从前述岩石地球化学特征可以看出,穆尔尕布辉长岩贫硅富镁(SiO_2 含量为46.5%~49.94%, MgO 含量为9.01%~15.67%),属于钙碱性-高钾钙碱性系列,且具有较高的Mg[#]值(63.6~72.7)和Cr含量(307×

10^{-6} ~ 1180×10^{-6}),Sc元素含量介于 29.2×10^{-6} ~ 49.8×10^{-6} ,Co元素含量为 42.6×10^{-6} ~ 65.4×10^{-6} ,这些特征表明,辉长岩的母岩浆不可能为下地壳镁铁质岩石的部分熔融,而是起源于地幔(Fery et al., 1978)。

岩体以富集轻稀土、贫重稀土元素,富集大离子亲石元素(Rb、Ba、U),而亏损高场强元素(Zr、Hf、Ti)为特征。这种地球化学特征的形成机制主要有强烈的地壳混染或由于俯冲带流体交代作用而

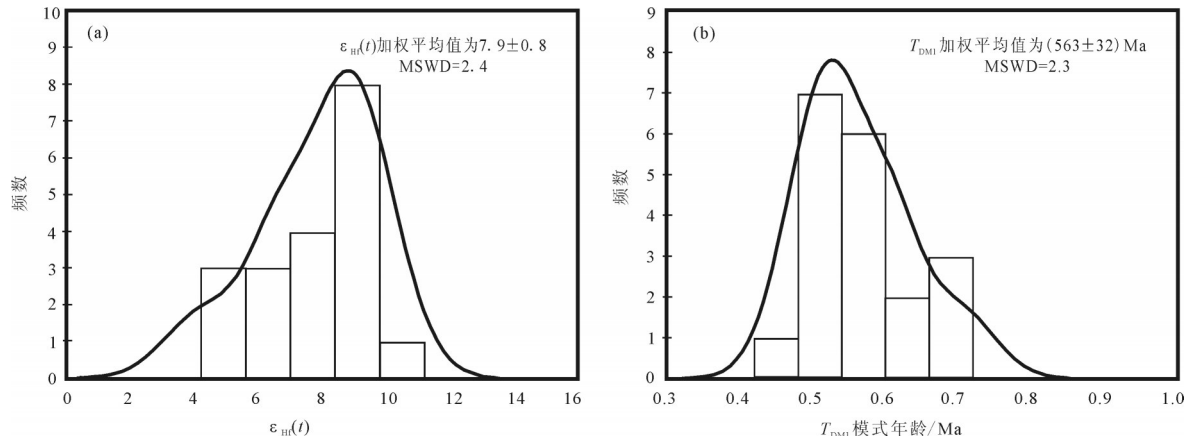


图7 穆尔尕布辉长岩锆石 $\epsilon_{\text{Hf}}(t)$ 值柱状分布图(a)和一阶段Hf模式年龄(b)

Fig.7 Columnar distribution of $\epsilon_{\text{Hf}}(t)$ values of zircons (a) and one-stage Hf model age (b) from Murgab gabbro

形成的富集地幔部分熔融(Yan et al., 2008)。 Nb/U 、 Ta/U 和 Ce/Pb 元素比值通常可以作为判断地壳混染的参考指标。辉长岩样品中 Nb/U 、 Ta/U 和 Ce/Pb 分别为37~66、2.8~4.9和9.6~13.6,与地壳($\text{Nb}/\text{U} \approx 12.1$ 、 $\text{Ta}/\text{U} \approx 1.1$ 和 $\text{Ce}/\text{Pb} \approx 4.1$) (Taylor and McLennan, 1995)相比,各项指标明显高于后者。此外,辉长岩锆石 $^{176}\text{Hf}/^{177}\text{Hf}$ 初始值为0.282752~0.282916,对应的 $\epsilon_{\text{Hf}}(t)$ 为4.8~12.1,均为正值,加权平均值为 8.1 ± 1.5 。表明岩体的母岩浆均起源于亏损地幔源区,且在上升过程中很少受壳源物质的混染。因此,认为穆尔尕布辉长岩的地球化学特征可能与岩浆源区受到俯冲带流体或熔体交代作用有关。俯冲带流体交代作用的过程为俯冲洋壳脱水,产生富集LILEs的流体进入上覆地幔楔,使地幔楔部分熔融,形成消减带岩浆(Eiler et al., 2000; Grove et al., 2003)。与正常岛弧玄武岩相比,具有富 Nb 和较低的LREE/HREE比值,较高的 P_2O_5 、 TiO_2 、 Zr 、 Sc 、 V 值的特点。研究区辉长岩的地球化学特征明显不同于熔体交代地幔楔形成的岩石,岩石贫K、富集LILEs,以及低的 Zr/Y 比值反映了流体交代地幔楔的源区特征(Davies et al., 1992; Arculus, 1994)。

与辉长岩空间共生的闪长岩以高硅、富碱($\text{Na}_2\text{O} > \text{K}_2\text{O}$)、贫 MgO 为特征,基性组分明显偏低,属于低钾(拉斑)系列;其 $\text{Cr}(10.5 \times 10^{-6} \sim 27.0 \times 10^{-6})$ 和 $\text{Ni}(10.4 \times 10^{-6} \sim 38.1 \times 10^{-6})$ 含量偏低, $\text{Mg}^{\#}$ 值介于39.2~53.8,表明闪长岩并非起源于幔源原始岩浆。闪长岩中结晶锆石的 $^{176}\text{Hf}/^{177}\text{Hf}$ 初始值为0.282752~

0.282916,对应的 $\epsilon_{\text{Hf}}(t)$ 介于6.4~10.0,加权平均值为 7.9 ± 0.8 ,结合其Hf模式年龄(T_{DM1} 为391~672 Ma),表明闪长岩的原始岩浆起源于早古生代或新元古代从亏损地幔分异出来的新生下地壳部分熔融。

5.3 构造环境及地质意义

穆尔尕布辉长岩-闪长岩类位于中帕米尔地体南缘、Rushan-Pshart缝合带中,形成时代为晚三叠世(232 Ma),属于低钾(拉斑)系列、钙碱性-中钾钙碱性系列,地球化学特征显示富Al低Ti,相对富集大离子亲石元素(LILEs),稀土元素总量高,明显富集LREE,亏损HREE和高场强元素(HFES),且辉长岩的 $\text{Zr/Y} < 4$,指示岛弧玄武岩的特征(Pearce, 1982; 汪云亮等, 2001; 孙书勤, 2003)。辉长岩和闪长岩的正的 $\epsilon_{\text{Hf}}(t)$ 值和其俯冲流体交代地幔楔的源区特征,也说明其形成于岛弧环境。

Rushan-Pshart带是中帕米尔和南帕米尔地体之间的板块缝合带,关于该缝合带的构造演化,前人已经开展了相关研究(Pashkov and Shvol'man, 1979; Burtman and Molnar, 1993; Leven, 1995; Schwab et al., 2004; Burtman, 2010; Angiolini et al., 2013)。普遍认为,目前沿Rushan-Pshart缝合带向南倾的逆冲断裂可以反映Rushan洋盆闭合过程中洋壳俯冲极性(Burtman and Molnar, 1993; Leven, 1995)。Rushan洋盆的规模也存在争议,其为与古特提斯洋是否为统一的大洋?大多数学者认为Rushan-Pshart缝合带代表中帕米尔和南帕米尔之间的规模相对较小的局限洋盆,主要依据是缝合带

两侧缺少大规模与俯冲相关的弧岩浆活动(Schwab et al., 2004; Burtman, 2010; Lukens et al., 2012; Angiolini et al., 2013)。关于洋盆闭合的时限,多数观点支持在晚侏罗世—早白垩世(Pashkov and Shvols'man, 1979, 1990; Burtman and Molnar, 1993; Schwab et al., 2004),也有学者认为 Rushan 洋盆在晚三叠世基梅里造山运动过程中闭合的。本文对中帕米尔地体南缘的穆尔尕布辉长岩-闪长岩开展岩石学、地球化学及锆石 LA-ICP-MS 法 U-Pb 定年和 Hf 同位素研究,结果表明,岩体的形成时代约为 232 Ma,其地球化学特征表明岩体可能形成于 Rushan 洋向北俯冲构造环境下的岛弧环境。结合区域地质资料,如在东南帕米尔识别出强变形的三叠纪地层中发育区域不整合,上覆早侏罗世陆源碎屑沉积,认为 Rushan 洋盆闭合时间晚于 232 Ma,在晚三叠世—早侏罗世期间。

6 结 论

(1) 帕米尔地区穆尔尕布辉长岩-闪长岩 LA-ICP-MS 锆石 U-Pb 年龄分别为 (231.5 ± 1.9) Ma 和 (232.0 ± 1.5) Ma, 代表其形成时代为晚三叠世早期。辉长岩的锆石 $\epsilon_{\text{Hf}}(t)$ 为 4.8~12.1, 加权平均值为 8.1 ± 1.5 。

(2) 地球化学特征显示岩体属于低钾拉斑系列-中钾钙碱性系列,富集 LILE 和 LREE, 亏损 HFES。辉长岩的母岩浆均起源于亏损地幔源区,且在上升过程中很少受壳源物质的混染,闪长岩的原始岩浆起源于早古生代或新元古代从亏损地幔分离出来的新生下地壳部分熔融。

(3) 穆尔尕布岩体可能形成于岛弧环境,晚三叠世 Rushan 洋陆俯冲尚未结束,表明洋盆闭合时限晚于 232 Ma。

致谢: 锆石 LA-ICP-MS U-Pb 定年测试得到中国地质调查局西安地质调查中心靳梦琪和汪双的热情帮助;匿名审稿专家和责任编辑对论文提出了建设性意见和建议,在此一并表示衷心感谢。

注释

①苏联国家地质委员会. 1956. 苏联 1:20 万区域地质图,图幅号 J43-XXI.

Reference

Angiolini L, Zanchi A, Zanchetta S, Nicora A, Vezzoli G. 2013. The

- Cimmerian geopuzzle: New data from South Pamir[J]. *Terra Nova*, 25, 352–360.
- Arculus R J. 1994. Aspects of magma genesis in arcs[J]. *Lithos*, 33: 189–208.
- Ballard J R, Palin J M, Williams I S. 2001. Two ages of porphyry intrusion resolved for the super-giant Chuquicamata copper deposit of northern Chile by LA-ICP-MS and SHRIMP[J]. *Geology*, 9:383–386.
- Blichert-Toft J and Albarede F. 1997. The Lu-Hf isotope geochemistry of chondrites and the evolution of the mantle-crust system[J]. *Earth Planet. Sci. Lett.*, 148: 243–258.
- Burtman V S and P Molnar. 1993. Geological and geophysical evidence for deep subduction of continental crust beneath the Pamir[J]. *Geol. Soc. Am. Spec. Pap.*, 281, 1–76.
- Davies J H, Stevenson D J. 1992. Physical model of source region of subduction zone volcanics[J]. *Journal of Geophysical Research*, 97: 2037–2070.
- Ducea M N, Lutkov V, Minaev V T, Hacker B, Luffi P, Metcalf J. 2003. Building the Pamirs: the view from the underside[J]. *Geological Society of America*, 31 (10): 849–852.
- Eiler J M, Crawford A J, Elliott T R, Farley K A, Valley J W, Stolper E M. 2000. Oxygen isotope geochemistry of oceanic arc lavas[J]. *Journal of Petrology*, 41:229–256.
- Frey F A, Prinz M. 1978. Ultramafic inclusions from San Carlos, Arizona: petrologic and geochemical data bearing on their petrogenesis[J]. *Earth and Planetary Science Letters*, 38(1):129–176.
- Griffin W L, Pearson N J, Belousova E, Jackson S E, Achterbergh E V. 2000. The Hf isotope composition of cratonic mantle: LAM-MC-ICPMS analysis of zircon megacrysts in kimberlites[J]. *Geochimica et Cosmochimica Acta*, 64: 133–147.
- Grove T L, Elkins Tanton L T, Parman S W, Chatterjee N, Müntener O, Gaetani G A. 2003. Fractional crystallization and mantle melting controls on calc-alkaline differentiation trends[J]. *Contributions to Mineralogy and Petrology*, 145(5): 515–533.
- Hong Jun, Ji Wenhua, Zhang Huishan, Yao Wenguang, Meng Guanglu, Wang Bin, Lv Pengrui, Yang Bo. 2014. Zircon SHRIMP U-Pb dating, geochemistry and tectonic implications of the Qieshijiebie gabbro on the northern margin of South Pamir[J]. *Geological Bulletin of China*, 33(6):820–829(in Chinese with English abstract).
- Hong Jun, Ji Wenhua, Zhang Huishan, Yao Wenguang, Fan Baoheng, Liu Mingyi, Luo Yanjun. 2015. LA-ICP-MS zircon U-Pb dating, geochemistry and tectonic implications of the Dugeli Alkali-rich porphyries on the eastern margin of Pamir[J]. *Acta Geologica Sinica*, 89(9):1463–1654(in Chinese with English abstract).
- Horn I, Rudnick R L, McDonough W F. 2000. Precise element and

- isotope ratio determination by simultaneous solution nebulization and LA-ICP-MS: Application to U-Pb geochronology[J]. *Chemical Geology*, 167:405-425.
- Kosler J, Fonneland H, Sylvester P. 2002. U-Pb dating of detrital zircons for sediment provenance studies—acomparison of LA-ICP-MS and SIMS techniques[J]. *Chemical Geology*, 182: 605-618.
- Leven E Y. 1995. Permian and Triassic of the Rushan-Pshart zone (Pamir) [J]. *Riv. Ital. Paleontol. Stratigr.* 101, 3-16.
- Ludwing K R. 2003. Isoplot 3.0—A geochronological toolkit for Microsoft Excel[J]. Berkeley Geochronological Center, Spec. Pub., (4):1-70.
- Lukens C E, Carrapa B, Singer B S, Gehrels G E. 2012. Miocene exhumation of the Pamir revealed by detrital geothermochronology of Tajikstan rivers[J]. *Tectonics* 31,12.
- Matte P, Tapponnier P, Arnaud N, Bourjot L, Avouac J P, Vidal P, Liu Q, Pan Y, Wang Y. 1996. Tectonics of Western Tibet, between the Tarim and the Indus[J]. *Earth Planet. Sci. Lett.* 142,311-330.
- Pashkov B R, Budanov V I. 1990. The tectonics of the zone of intersection between the Southeastern and southwestern Pamir[J]. *Geotectonics* 24, 246-253 (in Russian).
- Pashkov B R, Shvol'man V A. 1979. Rift margins of Tethys in the Pamirs[J]. *Geotectonics* 13, 447-456.
- Pearce J A. 1984. Trace element discrimination diagram for tectonic interpretation of granitic rocks[J]. *Petrology*, 25: 656-682.
- Robinson A C, Yin An, Manning C E, Harrison T M, Zhang S H, Wang X F. 2004. Tectonic evolution of the northeastern Pamir: constraints from the northern portion of the Cenozoic Kongur Shan extensional system[J]. *Geol. Soc. Am. Bull.*, 116: 953-974.
- Robinson A C, Yin An, Manning C E, Harrison T M, Zhang S H, Wang X F. 2007. Cenozoic evolution of the eastern Pamir: implications for strain accommodation mechanisms at the western end of the Himalayan-Tibetan orogen[J]. *Geol. Soc. Am. Bull.* 119, 882-896.
- Robinson A C, Ducea M, Lapen T J, 2012. Detrital zircon and isotopic constraints on the crustal architecture and tectonic evolution of the northeastern Pamir[J]. *Tectonics* 31, TC2016.
- Scherer E, Munker C and Mezger K, 2001, Calibration of the lutetium-hafnium clock[J]. *Science*, 293: 683-687.
- Schwab M, Ratschbacher L, Siebel W, McWilliams M, Minaev V, Lutkov V, Chen F, Stanek K, Nelson B, Frisch W, Wooden J L.2004. Assembly of the Pamirs: Age and origin of magmatic belts from the southern Tienshan to the southern Pamirs and their relation to Tibet[J]. *Tectonics* 23, TC4002.
- Sun Shuqin, Wang Yunliang, Zhang Chengjiang.2003.Discrimination of the tectonic settings of Basalts by Th, Nb, and Zr[J]. *Geological Review*, 49(1):40-47.
- Sun S S, McDonough W F.1989.Chemical and isotopic systematic of oceanic basalts: Implications for mantle composition and processes[C]//Saunders A D, Norry M J(eds.). *Magmatism in the Ocean Basins*[J]. Geological Society Special Publication,42:313-345.
- Taylor S R and Mc Lennan S. 1995. The geochemical composition of the continental crust [J]. *Reviews of Geophysics*, 33: 241-265.
- Vavra G, Gebauer D, Schmid R. 1996. Multiple zircon growth and recrystallization during polyphase Late Carboniferous to Triassic metamorphism in granulites of the Ivrea Zone: Anion microprobe study[J]. *Contrib. Mineral. Petrol.*, 122: 337-358.
- Wang Yunliang, Zhang Chengjiang, Xiu Shuzhi. 2001. Th/Hf-Ta/Hf identification of tectonic setting of basalts[J]. *Acta Petrologica Sinica*, 17 (3): 413-421(in Chinese with English abstract).
- Wu Yuanbao and Zheng Yongfei. 2004. Genesis of zircon and its constraints on inter pretation of U-Pb age[J]. *Chinese Science Bulletin*, 49(15): 1554-1569(in Chinese with English abstract).
- Yin An, Harrison T M.2000. Geologic evolution of the Himalayan-Tibetan orogen[J]. *Annu. Rev. Earth Planet. Sci.*, 28, 211-280.
- Yan Jun, Chen Jiangfeng, Xu Xisheng. 2008. Geochemistry of Cretaceous mafic rocks from the Lower Yangtze region, eastern China: characteristics and evolution of the lithospheric mantle [J]. *Journal of Asian Earth Sciences*, 33: 177-193.
- Yan Yi, Lin Ke, Li Zi'an. 2003. Provenance tracing of sediments by means of synthetic study of shape, composition and chronology of zircon[J]. *Geotectonica et Metallogenesis*, 27(2): 184-190.
- Yuan H L, Gao S, Liu X M et al. 2004. Accurate U-Pb age and trace element determinations of zircon by laser ablation-inductively coupled plasma mass spectrometry[J]. *Geostandards and Geoanalytical Reaerch*,28(3):353-370.

附中文参考文献

- 洪俊,计文化,张辉善,姚文光,孟广路,王斌,吕鹏瑞,杨博. 2014. 南帕米尔北缘切突界别辉长岩 LA-ICP-MS 锆石 U-Pb 定年、地球化学特征及其地质意义[J]. *地质通报*, 33(6): 820-829.
- 洪俊,计文化,张辉善,姚文光,范堡程,刘明义,罗彦军. 2015. 帕米尔东缘杜格里富碱斑岩锆石 U-Pb 定年、地球化学特征及构造意义[J]. *地质学报*, 89(9): 1463-1654.
- 孙书勤,汪云亮,张成江. 2003. 玄武岩类岩石大地构造环境的 Th、Nb、Zr 判别[J]. *地质论评*, 49(1): 40-47.
- 汪云亮,张成江,修淑芝. 2001. 玄武岩类形成的大地构造环境的 Th/Hf-Ta/Hf 图解判别[J]. *岩石学报*, 17(3): 413-421.
- 吴元保,郑永飞. 2004. 锆石成因矿物学研究及其对 U-Pb 年龄解释的制约[J]. *科学通报*, 49(16) : 1589-1604.
- 闫义,林柯,李自安. 2003. 利用锆石形态、成分组成及年龄分析进行沉积物源区示踪的综合研究[J]. *大地构造与成矿学*, 27(2): 184-190.